FEBS Letters 453 (1999) 90–94 FEBS 22159

Energetics of the proposed rate-determining step of the glyoxalase I reaction

Isabella Feierberg[a], Alexander D. Cameron[b], Johan Åqvist[a,*]

[a] *Department of Cell and Molecular Biology, Uppsala University, Box 596, S-751 24 Uppsala, Sweden*
[b] *Structural Biology Laboratory, Department of Chemistry, University of York, Heslington, York YO1 05DD, UK*

Received 28 April 1999; received in revised form 14 May 1999

Abstract The proposed rate-limiting step of the reaction catalyzed by glyoxalase I is the proton abstraction from the C1 carbon atom of the substrate by a glutamate residue, resulting in a high-energy enolate intermediate. This proton transfer reaction was modelled using molecular dynamics and free energy perturbation simulations, with the empirical valence bond method describing the potential energy surface of the system. The calculated rate constant for the reaction is approximately 300–1500 s^{-1} with Zn^{2+}, Mg^{2+} or Ca^{2+} bound to the active site, which agrees well with observed kinetics of the enzyme. Furthermore, the results imply that the origin of the catalytic rate enhancement is mainly associated with enolate stabilization by the metal ion.

Key words: Enzyme mechanism; Molecular dynamic; Free energy perturbation; Empirical valence bond

1. Introduction

Glyoxalase I (GlxI) catalyzes the formation of *S*-D-lactoylglutathione from the non-enzymatically formed hemithioacetal of methylglyoxal and reduced glutathione. This is the first of two enzymatic steps in the glyoxalase system in which toxic methylglyoxal is converted to D-lactic acid (Fig. 1). Though methylglyoxal appears to be the most physiologically relevant substrate, the system can catalyze analogous reactions with other 2-oxoaldehydes [1]. GlxI is a zinc metalloenzyme with an absolute requirement of metal ions for activity. Recently, the crystal structure of the dimeric human GlxI was solved [2], which shows a zinc ion present in each of the two identical active sites. The ion is coordinated by four protein residues (Gln-33, Glu-99, His-126 and Glu-172), whose arrangement can be considered as octahedral with the protein residues taking up four of the six coordination positions. To date, the structure of the wild-type enzyme has been solved in the presence of three different glutathione derivatives. The most interesting of these, from a mechanistic point of view, is the complex with *S*-(*N*-hydroxy-*N*-*p*-iodophenylcarbamoyl) glutathione (HIPC-GSH) [3]. This is a tight binding competitive inhibitor that mimics the stereoelectronic features of an enediol, the expected reaction intermediate. In this structure, the two oxygen atoms of the hydroxycarbamoyl function coordinate the zinc ion at the fifth and sixth coordination positions, implying that the reaction will also proceed via a metal coordinated *cis*-enediol. To arrive at the intermediate requires the abstraction of a proton from the substrate by a base on the protein. Based on structural analysis and site-directed mutagenesis studies, it seems that the most likely candidate for the base is Glu-172 [4]. Although this residue is a zinc ligand in two of the complexes, in the structure of the enzyme in complex with HIPC-GSH, the residue is displaced from the zinc coordination sphere.

The reaction mechanism via a *cis*-enediol intermediate resembles in some respects those of other enzyme-catalyzed enolization reactions, such as triose phosphate isomerase (TIM) [5], citrate synthase [6], mandelate racemase [7] and rubisco [8]. It is therefore of considerable interest to understand what general features an enzyme active site must possess in order to catalyze enolization reactions of this type and how these are dictated by the intrinsic energetics associated with such a chemistry [9]. The GlxI reaction is believed to be rate-limited by the initial proton abstraction described above from the C1 carbon atom, since a primary deuterium isotope effect of about three is observed when comparing phenylglyoxal with α-deuteriophenylglyoxal substrates [1]. The reaction has also been shown to be rather insensitive to the metal ion species bound in the active site [1,10,11]. All of Zn^{2+}, Mn^{2+}, Mg^{2+}, Co^{2+}, Ni^{2+} and Ca^{2+} show a significant catalytic activity, although Zn^{2+} is thought to be the catalytic ion in vivo since it has the highest binding affinity. This insensitivity to the metal contrasts with the optimization for specific metals observed in many other enzyme reactions [12].

In this letter, we report computer simulation studies of the first step of the GlxI reaction with the *S*-enantiomer of the substrate, utilizing a combination of the molecular dynamics (MD), empirical valence bond (EVB) and free energy perturbation (FEP) techniques [13,14]. Our main objective here is to analyze the energetics of what is probably the rate-limiting step on a detailed atomic level, in order to explain the basis of the catalytic rate enhancement. We also particularly address the issue of metal ion substitutions by carrying out calculations with Zn^{2+}, Mg^{2+} and Ca^{2+}.

2. Materials and methods

The reaction potential energy surface is represented by the EVB model which has been described in detail elsewhere [13,14]. This method describes a chemical reaction in terms of a number of resonance structures or valence bond (VB) states that represent different bonding arrangements and charge distributions of the reacting fragments. The energy of a given VB state i, corresponding to the diagonal element H_{ii} of the EVB hamiltonian is given by

$$H_{ii} = \varepsilon_i = V^{(i)}_{bond} + V^{(i)}_{angle} + V^{(i)}_{torsion} + V^{(i)}_{non-bond} + V^{(i)}_{rs} + V^{(i)}_{ss} + \alpha^{(i)} \quad (1)$$

The first term denotes the sum of Morse potentials for bonds and the second–fourth terms represent contributions from bond-angle bending, dihedral angle torsion and non-bonded van der Waals and

*Corresponding author. Fax: (46) (18) 53 69 71.
E-mail: aqvist@xray.bmc.uu.se

PII: S0014-5793(99)00703-6

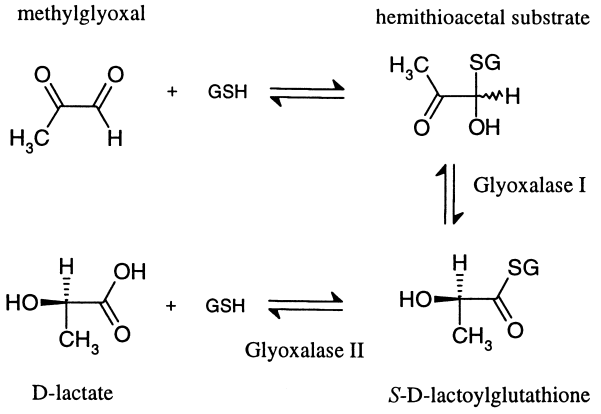

Fig. 1. Reactions of the glyoxalase system.

electrostatic interactions between the reacting groups. The fifth term is the interaction between the reacting fragments and the surroundings (enzyme and water) and the sixth term denotes the potential energy of the surrounding protein/solvent system. The last term of Eq. 1 is the intrinsic gas-phase energy of VB state i with all fragments at infinite separation [13,14].

The EVB method is combined with MD simulations whereby the free energy profile (potential of the mean force) along the reaction path can be mapped out using the FEP technique. For every configuration (coordinate set) of the system, the actual ground state energy is obtained by mixing the VB states through the off-diagonal hamiltonian elements and solving the corresponding secular equation. The free energy on this ground state surface is then obtained using a combined FEP and umbrella sampling approach [13,14]. The VB structures used in the present calculations are shown in Fig. 2, where partial atomic charges (obtained from semi-empirical AM1 calculations using the AMSOL program [15]) of the reacting fragments are also indicated. Equilibrium bond-lengths and dissociation energies for the reacting groups were taken from standard Morse potentials and AM1 calculations. The GROMOS87 force field was otherwise used in the calculations [16] together with the ion parameters of [17,18].

A key feature of the EVB method is that it allows calibration of the potential surface against relevant uncatalyzed reactions in solution. Here, the reaction free energy for the proton abstraction in water was calculated from the pK_a difference between the reacting groups, i.e. the substrate and glutamic acid (pK_a 4.1). Using linear free energy relationships, the effective free energy barrier for this reaction step in aqueous solution could be predicted in the same way as in [19]. The pK_a of the substrate was obtained using the experimental value (19.2) for the pK_a of acetone [20] as the starting point. The effect of the hydroxyl group substituent was earlier found to bring this pK_a down to 16.2 after correction for the number of equivalent protons [19]. The additional effect of the RS substituent was predicted using Benson's additivity rules [21] and the pK_a for the glutathione hemiacetal was thus estimated at 13.5. (The Benson scheme correctly predicts the effect of an RO substituent when compared to the experimental data in [22] as well as the pK_a of ethyl thioacetate relative to acetone, which is directly related to the thioester substrate of citrate synthase [23]. Although AM1-SM2 calculations also agree with the results for RO substituents, they give unrealistically large effects for sulfur substituents).

The estimated uncatalyzed activation free energy (which effectively includes zero-point energy and tunneling effects) is thus obtained as $\Delta G^{\ddagger}_{wat} = 22.1$ kcal/mol, with a corresponding standard reaction free energy of $\Delta G^{0}_{wat} = 12.8$ kcal/mol. The EVB calibration involves determining gas-phase free energy differences $\Delta\alpha_{ij}$ and off-diagonal matrix elements H_{ij} between pairs of VB states so that the resulting potential surface reproduces experimental reaction and activation free energies of the relevant reference reaction in solution. This calibration procedure thus involves simulations of the uncatalyzed reaction steps with the reacting fragments in water and fitting the above parameters so that calculated and observed free energies coincide. After calibration of the potential surface, these parameters are used without change to study the corresponding reaction in the solvated enzyme environment.

The simulations used the crystal structure of the enzyme in complex with HIPC-GSH [3] as the starting point, since this ligand is a good model for the enediol(-ate) intermediate. The reaction center was surrounded by an 18 Å sphere of water in the solution simulations and by a sphere of the same size, containing both protein and water, in the enzyme simulations. The protein atoms outside this sphere were restrained to their X-ray coordinates and interacted only via bonds across the boundary. A non-bonded cut-off of 10 Å was used together with multipole expansion for long range electrostatics [24]. The water surface was subjected to radial and polarization restraints as described elsewhere [25,26]. All calculations were carried out using the program Q [26]. Net charges were assigned to Arg-37, Glu-99, Arg-122, Lys-150 and Glu-172, since these residues are close to the reaction center, while ionizable groups near the sphere boundary were kept neutral to avoid unphysical dielectric effects [26]. 13 Internal crystal waters were retained in the starting structure because the solvation algorithm might miss the small cavities in which these water molecules are situated.

Initially, the protein-ligand complex was solvated and then heated from 1 to 300 K with all solute atoms restrained to their initial coordinates. At 300 K, the restraints were turned off and the system was equilibrated for 50 ps prior to data collection. The perturbations were carried out using 51 FEP steps, each comprising 5 ps of sampling of which the first 2 ps were discarded for equilibration. An MD time-step of 1 fs was used in all calculations.

In the Zn^{2+} simulation, two restraints were applied during the perturbation. The $N\varepsilon$ of His-126 was held at a 2.1 Å distance from the zinc ion center with a force constant of 100 kcal/(mol Å^2) (simulating the partly covalent character of the *d*-orbital-nitrogen interaction) and the side-chain carbonyl oxygen of Gln-33 was restrained to the ion center at 2.1 Å, with a weaker 10 kcal/(mol Å^2) force constant to ensure a reasonable coordination structure. In the Mg^{2+} and Ca^{2+} simulations, no restraints were used.

3. Results

The result of calibrating the uncatalyzed proton abstraction, by a glutamate residue in solution, against experimental

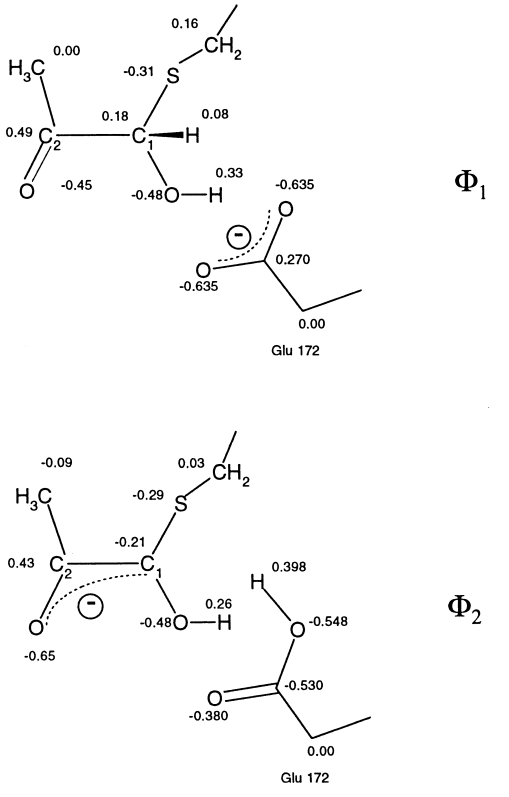

Fig. 2. EVB states and partial charges used in the calculations.

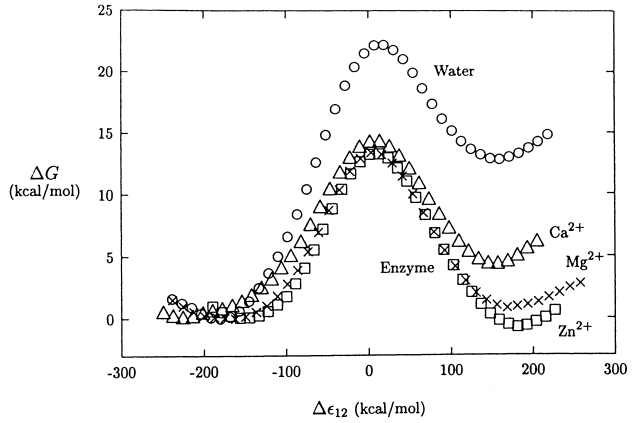

Fig. 3. Calculated free energy profiles for the proton abstraction by glutamate in solution and in GlxI with Zn^{2+}, Mg^{2+} and Ca^{2+} bound to the active site. The reaction coordinate $\Delta\varepsilon_{12}$ denotes the energy difference between the VB states Φ_1 and Φ_2 [13,14].

data is shown as the top free energy curve in Fig. 3. Already, the solution energetics of the process suggest that it is not enough for the enzyme to just reduce the activation of this reaction step barrier without stabilization of the enolate intermediate, since the reaction free energy deriving from the pK_a difference between glutamic acid and the substrate C1 carbon is quite high. That is, if subsequent proton transfers would be initiated from a state (the enolate species) that is about 13–14 kcal/mol above the ES complex, an overall turnover rate of $\sim$1500 s^{-1} [27] would be impossible to attain.

The corresponding free energy profiles for the enzyme reaction with different catalytic metal ions are also shown in Fig. 3. It is immediately evident from these free energy curves that the enzyme exerts a large stabilization of both the transition state (TS) and the enolate species resulting from proton abstraction. While the TS is found to be stabilized by about 9 kcal/mol with Mg^{2+} or Zn^{2+} and 8 kcal/mol with Ca^{2+}, the free energy of the enolate is reduced by 12 and 13.6 kcal/mol with Mg^{2+} or Zn^{2+}, respectively, and by about 10 kcal/mol with Ca^{2+} bound to the active site. It is interesting to note that the three ions give very similar activation free energies, corresponding to a rate constant for this enzymatic step of approximately 300–1500 s^{-1}, which is in good agreement with the observed rate of GlxI [27] (as noted above, deuterium isotope effect experiments suggest that this is indeed the rate-limiting step of the enzyme [1]).

The observed stabilization of the charged high-energy enolate intermediate is found to be the main source of catalysis for the proton abstraction step. That is, by reducing ΔG^0 for this reaction step, the associated activation barrier is lowered as a consequence of the correlation (linear free energy relationship) between ΔG^0 and $\Delta G^{\ddagger}$. For instance, in the Mg^{2+}-loaded enzyme, the lowering of ΔG^0 accounts for 7 kcal/mol of the barrier reduction while the remaining 2 kcal/mol originate from reduction of the reorganization free energy. This result is obtained as described in [19] by carrying out a 'hypothetical' recalibration of the uncatalyzed reaction free energy so that it coincides with the calculated value in the enzyme. If the resulting hypothetical (uncatalyzed) barrier then also coincides with the calculated activation energy in the enzyme, then, the lowering of ΔG^0 explains the entire catalytic effect. However, in this case (see also [19]), a residual barrier reduction of $\Delta\Delta G^{\ddagger} \approx 2$ kcal/mol remains, which is not due to the lowering of ΔG^0. This latter type of catalytic rate enhancement can be interpreted as a pure TS 'stabilization' which originates from reduction of the reorganization energy. The idea that enzymes may be able to reduce reorganization energies has been discussed by several workers [9,28–30]. That this effect is real has also been demonstrated by microscopic calculations [19,31,32]. In the context of enzymes catalyzing proton abstractions from carbon acids, Gerlt and Gassman [9] and Cleland and Kreevoy [33] have suggested that so-called low-barrier hydrogen bonds (LBHBs) may contribute significantly to the catalytic effect, although the notion that LBHBs would provide as much as 20 kcal/mol stabilization has often been criticized (see, e.g. [34]). In GlxI, the observed stabilization of the enolate intermediate is mainly achieved by the metal rather than by a hydrogen bond.

With a reliable computational model that includes all relevant components of the catalytic system (enzyme, substrate, water, cofactors) and that can quantitatively predict the rate constant observed experimentally, it becomes possible to dissect the source of catalysis in detail. That is, all interaction energies of interest can be monitored and averaged over the simulation trajectories to provide an essentially complete picture of the role of different interactions for catalysis. This is the main strength of computer simulation for studying enzyme reactions, since experimental methods are usually not able to distinguish important contributions to catalysis from each other. A case in point here is, e.g., the role of the metal ion in the differential stabilization of reactants and products in our proton abstraction step.

An energetic analysis of the uncatalyzed reaction step in water and in GlxI, in fact, clearly reveals that the metal (Mg^{2+}, Ca^{2+} and Zn^{2+}) is the key factor in stabilization of the enolate intermediate. In the uncatalyzed solution reaction, there is an unfavorable desolvation effect associated with charge delocalization as the negative charge migrates from the carboxylate moiety to the enolate ion. This effect is immediately apparent from the average electrostatic interaction energy between the reacting groups and their surroundings for the two states in Fig. 2. This interaction becomes about 30 kcal/mol more positive for the Φ_2 state than for Φ_1 in solution. In the enzyme, on the other hand, the corresponding 'desolvation' energy difference (including interactions with both the enzyme, water and metal) is reduced to less than 10 kcal/mol. It can be noted here that linear response approximation [35] would then predict a reaction free energy reduction contribution of $1/2(30-10) = 10$ kcal/mol from 'electrostatic solvation'. This agrees with our overall observed value (Fig. 3) and shows that electrostatic stabilization of the enolate is indeed the main source of catalysis (there is no significant contribution from the van der Waals energies). Furthermore, one finds that the metal ion, which is the main contributor to the interaction energy with the reacting groups, has electrostatic interactions of very similar magnitude with the reactant and product states. The reason for this appears to be the specific coordination structure around the metal ion. In the reactant state, the MD structure (not shown) has the negatively charged Glu-172 providing a monodentate ligand to the metal with one of its oxygens, while the enolate ion in the Φ_2 state can ligate the metal with both of its oxygens thus yielding a strong interaction with the negatively charged intermediate (Fig. 4). The active site structure, and particularly the metal coordination sphere, thus appears ideally suited to

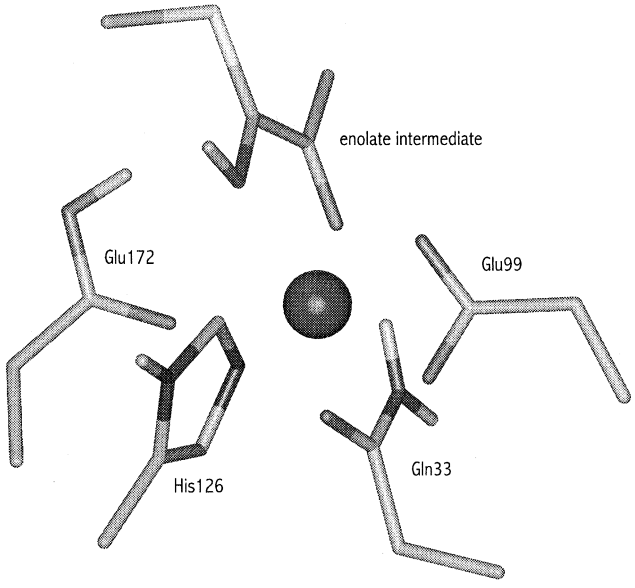

Fig. 4. MD average structure of the enolate species (Φ_2) in the active site with Mg^{2+} as a cofactor.

balance or level out the energetics of proton abstraction from the substrate hemiacetal.

4. Discussion

It is of considerable interest to try to understand the general features required by an enzyme active site that catalyze enolization reactions of the present type. The main obstacle, and reason for the low uncatalyzed turnover numbers, is that the carbon atoms from which proton abstraction must occur are very non-acidic (i.e. high pK_as). In the present case of GlxI, TIM [19,36] and citrate synthase [37] computational studies have identified electrostatic stabilization of the high-energy enolates as the key factor in catalysis. However, this stabilization can apparently be achieved by different structural or evolutionary solutions. While we have identified the active site metal in GlxI as the main source of enolate stabilization, the same effect is attained in TIM through interactions with Lys-12, His-95 and a water molecule. That is, TIM instead employs one net positive charge and two dipolar groups to stabilize the high-energy intermediate. More puzzling is the case of citrate synthase where only two dipolar groups (His-274 and a water molecule) seem to do the job [6,37], despite the fact that its thioester type substrate has even a slightly higher pK_a than acetone [23]. How this can be achieved remains to be explained. In the enolase superfamily (e.g. glucarate dehydratase and mandelate racemase), divalent metal ions are again employed to promote enolate stabilization. This is also the case in rubisco where the first reaction step involves enolization of the substrate. There, enolization appears to proceed in a similar manner to GlxI, the substrate is ligated to the catalytic Mg^{2+} ion and general base catalysis is presumably effected by the carbamylated Lys-201 (which is also a metal ligand) [8]. Further computer simulation studies of some of these other mentioned enzymes could hopefully provide us with a consistent energetic picture of enolization catalysis.

Another issue of interest in the general context of metal-assisted enzyme catalysis is the sensitivity or optimization for specific metal ion species [12]. In many metalloenzymes, the main role of the ion is to generate a reactive anionic nucleophile (e.g. RO^-) for a subsequent or concerted attack on the substrate and the metal is then also often involved in stabilization of developing a negative charge on the substrate accompanying the nucleophilic attack [12]. In these cases, optmization of the enzyme for a specific metal can result as a consequence of the following effect. The more electrophilic the metal is, the lower the pK_a of the ligated nucleophile becomes. But, if it becomes too low, the nucleophile anion will be 'trapped' as a metal ligand and not be labile enough for an attack on the substrate [12]. In GlxI, the situation is different. Here, the important consideration is not the pK_a of Glu-172 but the pK_a difference between Glu-172 and the substrate. Because of the proximity to the metal ion, the pK_as of both these zinc ligands are lowered relative to their values in solution and the pK_a difference is reduced as well (Fig. 3).

The charge of Glu-172 is more delocalized than, e.g., an RO^- ion which presumably makes its interaction with the ion relatively weaker. This, in combination with the efficient positioning of the two substrate oxygens as metal ligands, results in an almost perfect energy balance for proton abstraction to occur. It does, then, not seem so surprising that this balance can be retained with a number of different cations, provided that they do not distort the ligand coordination pattern drastically.

Although we have only considered what has been reported as the rate-limiting step here, there are several issues regarding the catalytic mechanism of GlxI that remain to be resolved. In particular, it is not yet clear whether Glu-172 effects all necessary proton transfers during the reaction or whether Glu-99 (located at the opposite side of the metal) is also involved. Mutation of Glu-172 to Gln completely abolishes enzyme activity [4], indicating that its function as a general base (at least for *S*-substrates) cannot be effected by any other residue. Moreover, mutation of Glu-99 to Gln also has a significant effect on catalysis, reducing the rate by a factor of 1000 [4] for a racemic substrate. This could either be interpreted such that it actually participates in some of the proton transfers or that Glu-99 is essential for maintaining the coordination sphere of the metal ion. An interesting observation is that reaction with the pure *R*-form of the substrate can equally well be catalyzed by GlxI which specifically always yields the *S*-product [38]. This may suggest that Glu-99 can replace the action of Glu-172 for the initial proton abstraction from *R*-substrates, since the labile C1 proton in the *R*-enantiomer is rather pointing towards Glu-99 and not Glu-172.

In summary, we have reported here MD/FEP/EVB simulations of the proposed rate-limiting step in GlxI. The computational model used is able to provide a detailed picture of the initial catalytic step. Both the activation free energy barrier obtained and its insensitivity to three different divalent metal ions agree with experimental kinetic data. The source of the catalytic rate enhancement has also been analyzed in some detail and has been found to derive mainly from the metal's ability to balance the energetics of the otherwise highly unfavorable proton abstraction from a very non-acidic carbon atom. Thus, the major contribution to the catalytic effect corresponds to a stabilization of the enolate intermediate although there is also a significant reduction of the reorganization energy of this reaction step, compared to the uncata-

lyzed process in aqueous solution. These features appear to be quite general as far as enzyme-catalyzed enolization reactions are concerned [19], although several other enzymes have found different structural solutions to the problem of enolate stabilization.

Acknowledgements: Support from the Swedish Foundation for Strategic Research (SSF/SBnet) and the NFR is gratefully acknowledged.

References

[1] Vander Jagt, D.L. (1989) in: Coenzymes and Cofactors (Dolphin, D., Poulson, R. and Avramovic, O., Eds.), Vol. 3A, pp. 597–641, John Wiley and Sons, New York.
[2] Cameron, A.D., Olin, B., Ridderström, M., Mannervik, B. and Jones, T.A. (1997) EMBO J. 12, 3386–3395.
[3] Cameron, A.D., Olin, B., Ridderström, M. and Mannervik, B. (1999) (submitted).
[4] Ridderström, M., Cameron, A.D., Jones, T.A. and Mannervik, B. (1998) J. Biol. Chem. 273, 21623–21628.
[5] Davenport, R.C., Bash, P.A., Seaton, B.A., Karplus, M., Petsko, G.A. and Ringe, D. (1991) Biochemistry 30, 5821–5826.
[6] Wlassics, I.D. and Anderson, V.E. (1989) Biochemistry 28, 1627–1633.
[7] Gulick, A.M., Palmer, D.R.J., Babbitt, P.C., Gerlt, J.A. and Rayment, I. (1998) Biochemistry 37, 14358–14368.
[8] Taylor, T.C. and Andersson, I. (1997) J. Mol. Biol. 265, 432–444.
[9] Gerlt, J.A. and Gassman, P.G. (1993) J. Am. Chem. Soc. 115, 11552–11568.
[10] Mannervik, B., Lindström, L. and Bartfai, T. (1972) Eur. J. Biochem. 29, 276–281.
[11] Uotila, L. and Koivusalo, M. (1975) Eur. J. Biochem. 52, 493.
[12] Åqvist, J. and Warshel, A. (1990) J. Am. Chem. Soc. 112, 2860–2868.
[13] Warshel, A. (1991) Computer Modeling of Chemical Reactions in Enzymes and Solutions, John Wiley and Sons, New York.
[14] Åqvist, J. and Warshel, A. (1993) Chem. Rev. 93, 2523–2544.
[15] Cramer, C.J. and Truhlar, D.G. (1992) Science 256, 213–217.
[16] van Gunsteren, W.F. and Berendsen, H.J.C. (1987) Groningen Molecular Simulation (GROMOS) Library Manual, Biomos B.V., Nijenborgh, Groningen.
[17] Åqvist, J. (1990) J. Phys. Chem. 94, 8021–8024.
[18] Åqvist, J. (1992) J. Mol. Struct. (Theochem.) 256, 135–152.
[19] Åqvist, J. and Fothergill, M. (1996) J. Biol. Chem. 271, 10010–10016.
[20] Chiang, Y., Kresge, A.J., Tang, Y.S. and Wirz, J. (1984) J. Am. Chem. Soc. 115, 631–635.
[21] Benson, S.W., Cruickshank, F.R., Golden, D.M., Haugen, G.R., O'Neal, H.E., Rodgers, A.S., Shaw, R. and Walsh, R. (1969) Chem. Rev. 69, 279–324.
[22] Guthrie, J.P. (1979) Can. J. Chem. 57, 1177–1185.
[23] Amyes, T.L. and Richard, J.P. (1994) J. Am. Chem. Soc. 114, 10297–10302.
[24] Lee, F.S. and Warshel, A. (1992) J. Chem. Phys. 97, 3100–3107.
[25] King, G. and Warshel, A. (1989) J. Chem. Phys. 91, 3647–3661.
[26] Marelius, J., Kolmodin, K., Feierberg, I. and Åqvist, J. (1999) (submitted).
[27] Ridderström, M., Cameron, A.D., Jones, T.A. and Mannervik, B. (1997) Biochem. J. 328, 231–235.
[28] Warshel, A. (1978) Proc. Natl. Acad. Sci. USA 75, 5250–5254.
[29] Albery, W.J. (1980) Ann. Rev. Phys. Chem. 31, 227–263.
[30] Cannon, W.R. and Benkovic, S.J. (1998) J. Biol. Chem. 273, 26257–26260.
[31] Yadav, A., Jackson, R.M., Holbrook, J. and Warhel, A. (1991) J. Am. Chem. Soc. 113, 4800–4805.
[32] Warshel, A., Hwang, J.K. and Åqvist, J. (1992) Faraday Discuss. 93, 225–238.
[33] Cleland, W.W. and Kreevoy, M.M. (1994) Science 264, 1887–1890.
[34] Guthrie, J.P. (1996) Chem. Biol. 3, 163–170.
[35] Åqvist, J. and Hansson, T. (1996) J. Phys. Chem. 100, 9512–9521.
[36] Bash, P.A., Field, M.J., Davenport, R.C., Petsko, G.A., Ringe, D. and Karplus, M. (1991) Biochemistry 30, 5826–5832.
[37] Mulholland, A.J. and Richards, W.G. (1997) Proteins 27, 9–25.
[38] Landro, J.A., Brush, E.J. and Kozarich, J.W. (1992) Biochemistry 31, 6069–6077.